Supporting Information for

Piezoelectric polarizations and valley-related multiple Hall effect in monolayer $TiAlX_3$ (X=Se, Te)

Jia Li[a*], Jianke Tian[b], Hengbo Liu[b], Yan Li[b], Linyang Li[b], Jun Li[b], Guodong Liu[b], Junjie Shi[c]

[a]*College of Science, Civil Aviation University of China, Tianjin 300300, People's Republic of China*

[b]*School of Science, Hebei University of Technology, Tianjin 300401, People's Republic of China*

[c]*State Key Laboratory for Artificial Microstructures and Mesoscopic Physics, School of Physics, Peking University Yangtze Delta Institute of Optoelectronics, Peking University, 5 Yiheyuan Street, Beijing, 100871, People's Republic of China.*

* Corresponding author. *E-mail address*: lijia@cauc.edu.cn (J. Li).

Table. S1. The MAE (μeV), energy difference between AFM1, AFM2, AFM3 and FM ording ($meV/unit\ cell$), the Heisenberg exchange parameters J_1 and J_2 (meV) and T_c (K) for $TiAlSe_3$ and $TiAlTe_3$ monolayers.

$material$	MAE	ΔE_{AFM}	ΔE_{AFM}	ΔE_{AFM}	J_1	J_2
$TiAlSe_3$	43	34.06	14.27	29.11	4.40	-0.39
$TiAlTe_3$	468	23.61	8.42	13.58	7.80	-1.79

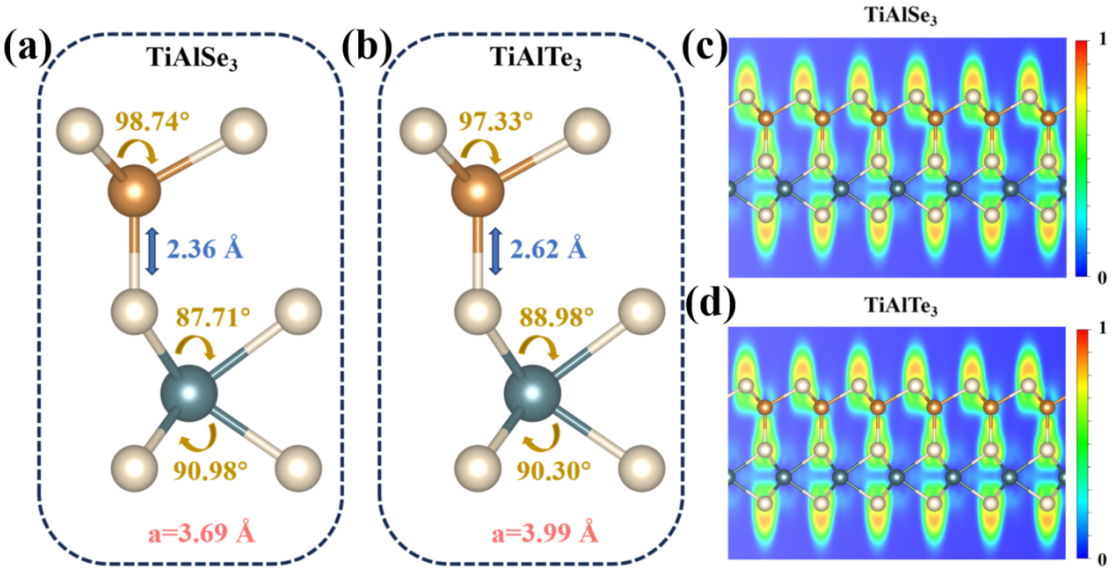

Fig. S1. The graphic representation of a unit cell with structural properties for (a) $TiAlSe_3$ and (b) $TiAlTe_3$ monolayers. The electron localization function of (c) $TiAlSe_3$ and (d) $TiAlTe_3$.

Under compressive strain, there are small negative frequencies (less than 0.50 cm^{-1}) at Γ point (along ΓM direction), which are provided by out-of-plane acoustic mode (ZA). Previous studies have shown that the lattice dynamics calculations based on DFPT have a persistent problem of non-vanishing frequencies of acoustic modes. This negative frequency could be caused by phonon-magnetic coupling or strong electron correlations and such a small value of negative frequencies can be ignored and thus the structure can be considered to be dynamically stable.

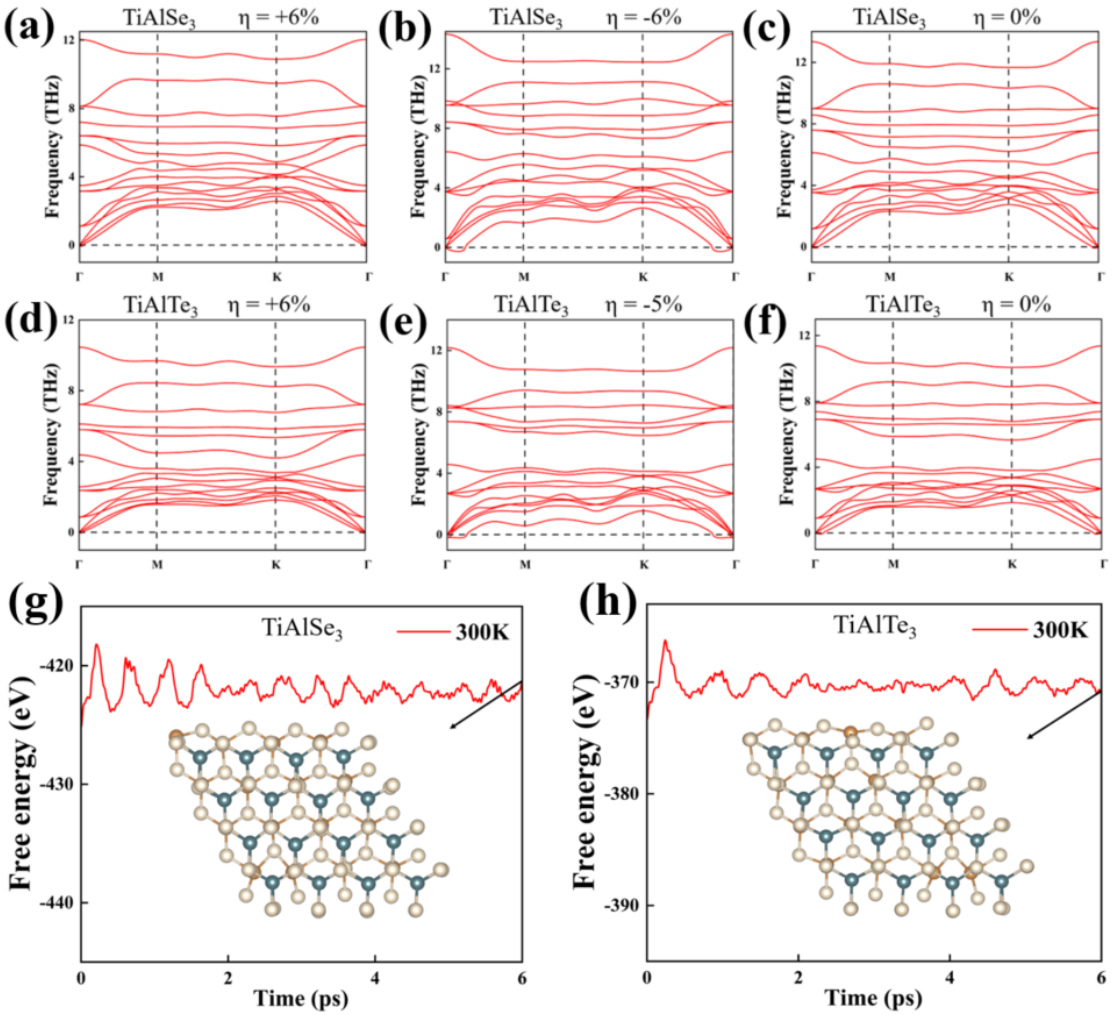

Fig. S2. (a)-(f) Biaxial strain-dependent phonon spectra of $TiAlSe_3$ and $TiAlTe_3$. The fluctuation of total energy and snapshots of geometric structures for (g) $TiAlSe_3$ and (h) $TiAlTe_3$ at 6 ps from AIMD simulations.

The breaking of inversion symmetry results in an unequal charge transfer, which is reflected by the drop of averaged potential and electrostatic potential gradient. The asymmetric average electrostatic potential along the z-axis shows the out-of-plane dipole moment and the inherent electric field k of system can be obtained from the slope of the plane average electrostatic potential between the outermost atoms. The intrinsic polarization implied by large out-of-plane dipole moment and the inherent electric field indicates the possible existence of good piezoelectric properties.

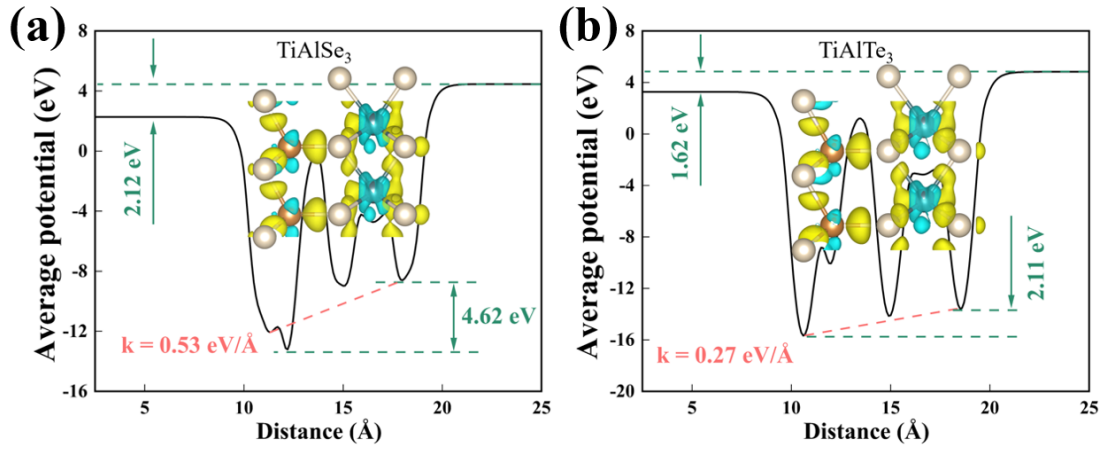

FIG. S3. The planar average electrostatic potential energy of $TiAlSe_3$ and $TiAlTe_3$.

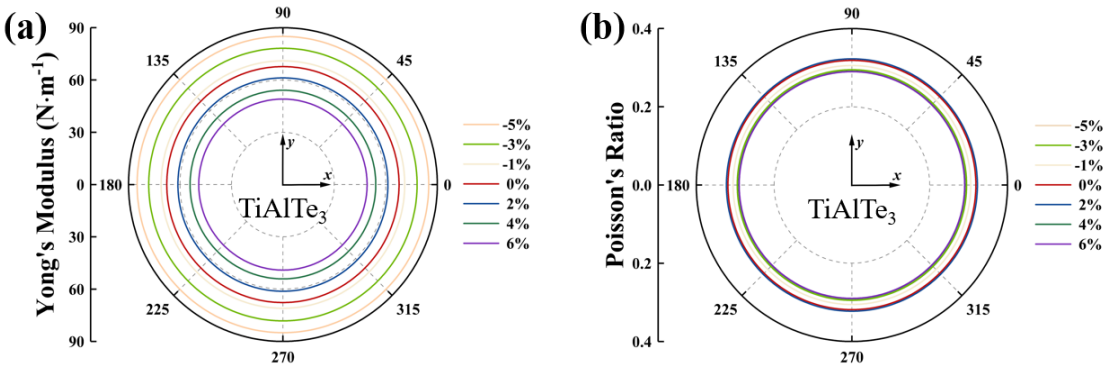

Fig. S4. (a) The Young's modulus and (b) Poisson's ratio for $TiAlTe_3$

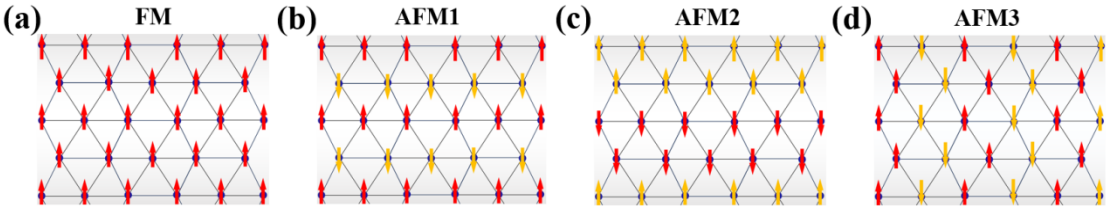

Fig. S5. (a) FM, (b) AFM1, (c) AFM2 and (d) AFM3 states of crystal structures, and the red (orange) arrow shows the direction of spin-up (spin-down).

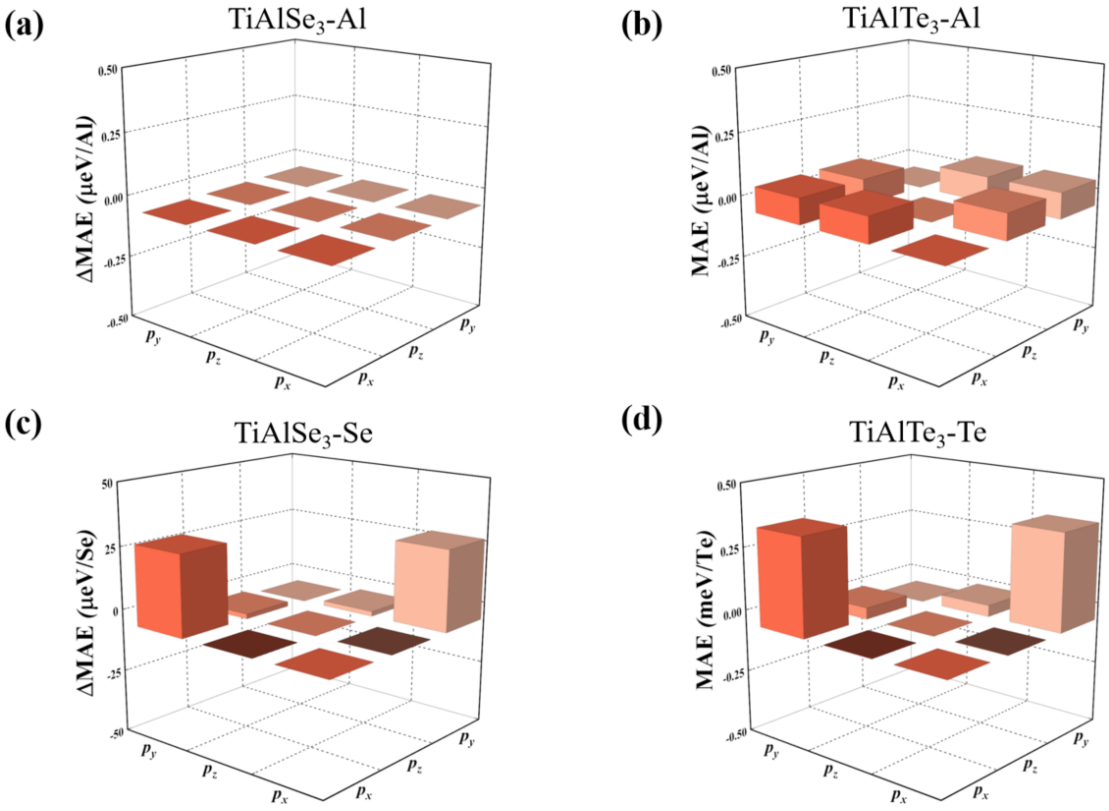

Fig. S6. The orbital-resolved MAE of (a),(b) Al and (a),(d) X atoms for $TiAlX_3$.

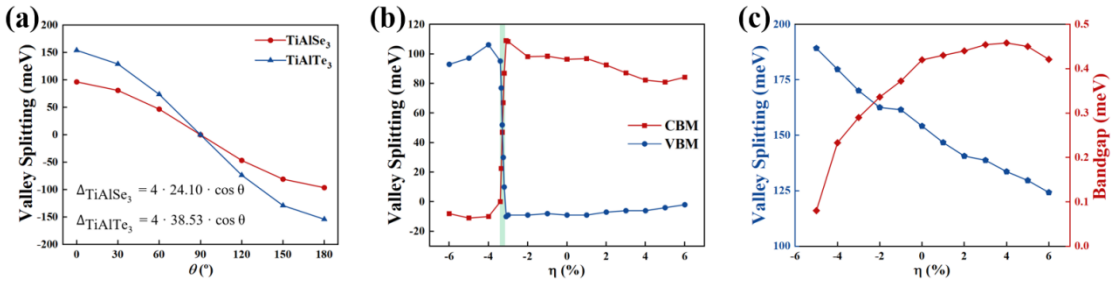

Fig. S7. (a) Valley polarization as the function of magnetization direction for $TiAlSe_3$ and $TiAlTe_3$, and the function is the corresponding cosine function. (b) Valley polarization in CBM and VBM of $TiAlSe_3$ under different biaxial strain. (c) Valley polarization in CBM and bandgap of $TiAlTe_3$ under different biaxial strain.

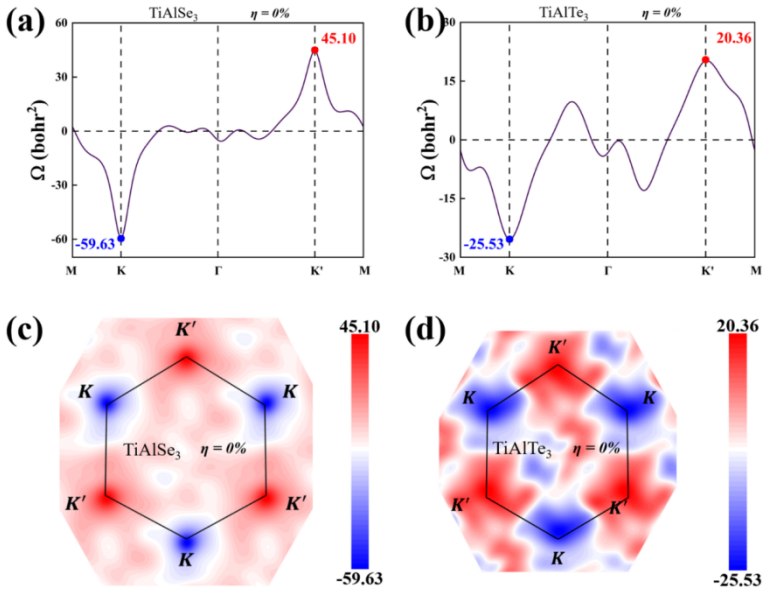

Fig. S8. (a) and (b) The Berry curvatures $\Omega(k)$ as the curve along the high-symmetry path with the unit of $Bohr^2$ for $TiAlSe_3$ and $TiAlTe_3$ monolayers. (c)-(d) Contour map of Berry curvatures in the k space for $TiAlSe_3$ and $TiAlTe_3$ monolayers.

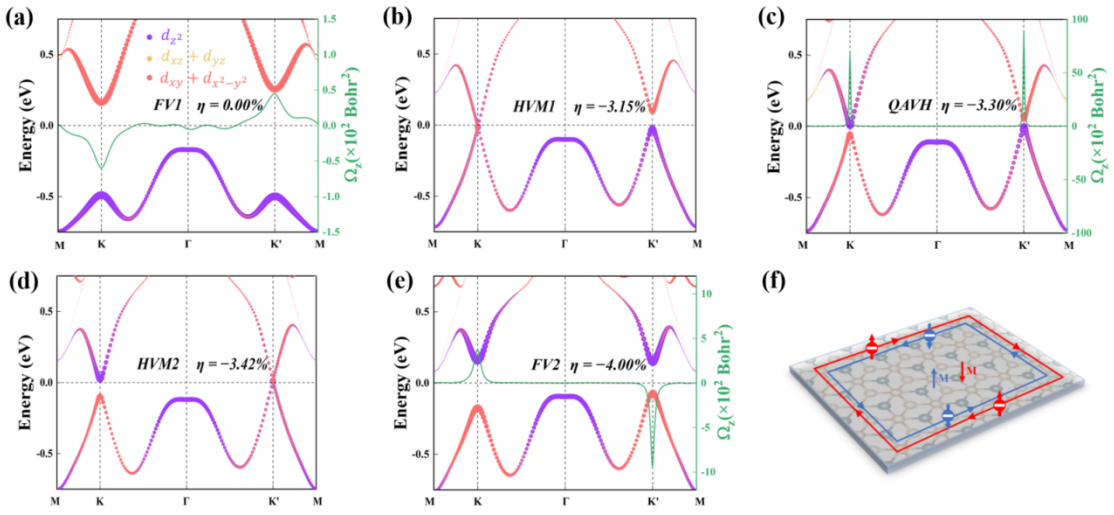

Fig. S9. (a)-(e) are the diagrams of the evolution of the electronic band structures with biaxial strains, and the green curves denote the Berry curvatures of the corresponding system. (f) Schematic diagram of QAVHE in $TiAlSe_3$. The red and blue represent the upper and lower spin channels, respectively.

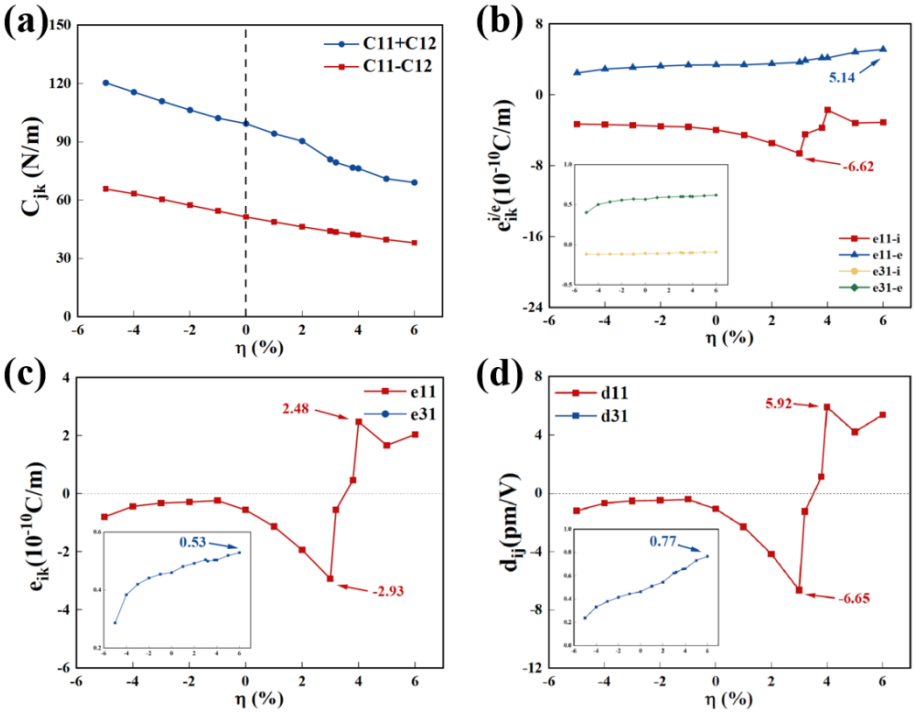

Fig. S10. (a) For $TiAlTe_3$, (a) the elastic constants C_{jk}, (b) piezoelectric stress coefficient e_{ik} along with the ionic contribution and electronic contribution, the piezoelectric stress coefficient e_{ik} and (d) piezoelectric coefficient d_{ij} as a function of strain.